



Study of the Top Quark Production Asymmetry and Its Mass and Rapidity Dependence in the Full Run II Tevatron Dataset

The CDF Collaboration

URL <http://www-cdf.fnal.gov>

(Dated: May 2, 2012)

We present a new measurement of the inclusive forward-backward $t\bar{t}$ production asymmetry, A_{FB} , and its rapidity and mass dependence. The measurements are performed with an integrated luminosity of 8.7 fb^{-1} of $p\bar{p}$ collisions, the full Tevatron dataset at $\sqrt{s} = 1.96 \text{ TeV}$, recorded with the CDF II Detector. In events containing a lepton, multiple jets, and large missing energy, we measure the asymmetry in the frame-invariant difference of the t and \bar{t} rapidities, Δy . Parton-level results are derived with a fully general multi-bin correction procedure assuming the acceptance and resolution of the SM NLO generator POWHEG. We derive the differential cross-section $d\sigma/d(\Delta y)$ and the inclusive asymmetry. The rapidity and mass dependence of the asymmetry are well fit by linear functions. We measure the slopes for both the detector-level and parton-level dependence and compare to the NLO standard model. p-values to the standard model are calculated for the slopes at the detector level.

Preliminary Results for Winter 2012 Conferences

I. INTRODUCTION

The creation of top quarks in $q\bar{q}$ annihilation is a unique test of pair-production in QCD at very large momentum transfer. The CDF and D0 collaborations have previously reported on forward-backward asymmetries in $q\bar{q} \rightarrow t\bar{t}$ production at $\sqrt{s} = 1.96$ TeV at the Fermilab Tevatron. This strong process is symmetric in production angle except for a small charge asymmetry ($\mathcal{O}(7\%)$) arising in higher order QCD [1]. Using samples of roughly 5 fb^{-1} , CDF measures parton level asymmetries of $A_{\text{FB}} = 0.158 \pm 0.074$ [2] in the lepton+jets channel and $A_{\text{FB}} = 0.42 \pm 0.16$ [3] in the dilepton channel. Combining the two CDF results gives $A_{\text{FB}} = 0.201 \pm 0.067$ [4]. This is in very good agreement with an independent D0 measurement of $A_{\text{FB}} = 0.196 \pm 0.065$ [5] in a similarly sized sample. CDF and D0 have performed simple differential measurements in the l +jets samples using two bins each in the proxy variables Δy and $M_{t\bar{t}}$. The two experiments agree on a large Δy dependence; CDF sees a large $M_{t\bar{t}}$ dependence, D0 a smaller, but statistically consistent, one.

These results have stimulated new work on the NLO QCD calculation which raised the level of the expected asymmetry somewhat ($6\% \rightarrow 7\%$), but not enough to account for the observations. More speculative consideration of the asymmetry invokes new interactions in the top sector [6]. In one group of models the gluon interferes with new axial s -channel objects arising from an extended strong gauge group or extra dimensions. In other models, light t -channel objects with flavor violating couplings create an asymmetry via a $u/d \rightarrow t$ flavor change into the forward Rutherford peak. Model-building must accommodate the apparent standard model consistency in the measured cross-section and $M_{t\bar{t}}$ spectrum. Other related phenomena, such as di-jet bumps, same-sign tops, etc. lead to corollary limits or new search modes at the Tevatron and LHC.

This paper reports a new study on the asymmetry in the lepton+jets sample at CDF, including the following new features:

- We use the complete Run II dataset of 8.7 fb^{-1} , and include a new data stream, μ +jet events collected with a \cancel{E}_T trigger. The total sample size is 2498 events, compared to 1260 in the 5.3 fb^{-1} analysis.
- The default $t\bar{t}$ signal model is the NLO POWHEG generator, which contains the QCD asymmetry expected in the standard model. We also add small corrections reflecting new results on the electroweak contributions to the asymmetry.
- The acceptance corrections used to propagate the data to the parton level incorporate the NLO POWHEG model, which is important in events with extra jets.
- Parton level shape corrections utilize a regularized unfolding algorithm rather than the matrix-inversion of the previous analysis. This allows a proper multi-binned measurement of the rapidity and mass dependence of the asymmetry, $A_{\text{FB}}(\Delta y)$ and $A_{\text{FB}}(M_{t\bar{t}})$.
- $A_{\text{FB}}(\Delta y)$ and $A_{\text{FB}}(M_{t\bar{t}})$ are found to be well-fit by a linear ansatz, and the slopes are compared to the NLO predictions.

II. MONTE CARLO MODELS AND EXPECTED ASYMMETRIES

A. Standard Model

	MC@NLO	POWHEG	MCFM
Inclusive	0.067	0.066	0.073
$ \Delta y < 1$	0.047	0.043	0.049
$ \Delta y > 1$	0.130	0.139	0.150
$M_{t\bar{t}} < 450 \text{ GeV}/c^2$	0.054	0.047	0.050
$M_{t\bar{t}} > 450 \text{ GeV}/c^2$	0.089	0.100	0.110

TABLE I: Asymmetry predictions of POWHEG, MC@NLO, and MCFM after applying electroweak corrections.

The standard model predictions for the top asymmetry referenced in this note are based on the next-to-leading-order (NLO) event generator POWHEG [7]. We have made extensive checks of POWHEG against the NLO generator

MC@NLO [8], as well as the NLO calculation of MCFM [9]. We find good consistency, as evidenced by Table I. There are sources of asymmetry from electroweak processes in the standard model that are not included in the Monte Carlo calculations [10, 11, 12]. These amount to an overall increase of the asymmetry of 26%, which is included in the predictions shown in Table I. All predicted asymmetries and Δy distributions in this note contain this electroweak correction to POWHEG.

There is some debate about the order of the denominator ($N(\Delta y > 0) + N(\Delta y < 0)$) in the calculation of the standard model asymmetry. Since we treat the POWHEG events in the same manner that we treat the data, the denominator in the POWHEG asymmetry calculation effectively uses the NLO cross section. Arguments have recently been made that it is appropriate to use the LO cross section instead in the denominator, as the numerator ($N(\Delta y > 0) - N(\Delta y < 0)$) is effectively a LO calculation. The use of the LO cross section in the denominator can result in a significant, although poorly defined, increase in the asymmetry prediction. The reasons for the level of increase in the denominator, the $t\bar{t}$ cross section, are well-understood, and have no connection to the causes of the asymmetry[13]. The LO cross section has a much larger scale dependence than the NLO cross section and its value additionally strongly depends on whether a LO or NLO PDF is used in its evaluation.

For the studies here, it is most straightforward to use the clearly defined and self-consistent prediction that results from POWHEG, modified by the electroweak corrections. The data results are available for comparison to calculations of any definition.

In order to test our analysis methodology in the case of a large asymmetry, we study two models incorporating massive axial color octets. Each provides a reasonable approximation of our data in presenting a forward-backward asymmetry comparable to our measurement, while also being comparable to the data in other important variables like the $t\bar{t}$ invariant mass, $M_{t\bar{t}}$.

The first model, Octet A, contains an axigluon with a mass of $2 \text{ TeV}/c^2$. This new particle is massive enough that the pole is not observed in the $M_{t\bar{t}}$ spectrum, but still creates an asymmetry via the interference between the off-shell axigluon and the SM gluon. The couplings are tuned ($g_V(q) = g_V(t) = 0$, $g_A(q) = 3$, $g_A(t) = -3$) to produce a parton-level asymmetry that is very close to the parton level asymmetry observed in the 5.3 fb^{-1} analysis.

The second model, Octet B, contains an axigluon with a smaller mass of $1.8 \text{ TeV}/c^2$ and the same couplings. This model does produce a small excess in the high tail of the $M_{t\bar{t}}$ spectrum, and produces an even larger asymmetry than Octet A.

Both models are produced using the LO MADGRAPH [14] Monte Carlo generator and are showered with PYTHIA [15] before being passed to our detector simulation and reconstruction software. We emphasize that these are not hypotheses, but, rather, controlled inputs for the study of potential biases and systematic uncertainties.

III. DETECTION, SELECTION, AND RECONSTRUCTION

The data sample is derived from 8.7 fb^{-1} of $p\bar{p}$ collisions at 1.96 TeV recorded with the CDF II detector. CDF II is a general purpose, azimuthally and forward-backward symmetric magnetic spectrometer with calorimetry and muon detectors [16].

CDF Run II Preliminary L = 8.7 fb^{-1}		
≥ 4 jets		
W+HF	241 \pm	78
Non-W	98 \pm	51
W+LF	96 \pm	29
Single Top	33 \pm	2
Diboson	19 \pm	3
Z+Jets	18 \pm	2
Total Background	505 \pm	123
$t\bar{t}$ 7.4pb	2037 \pm	277
Total Prediction	2542 \pm	303
Data	2498	

TABLE II: Sample composition.

This measurement uses $t\bar{t}$ candidate events in the “lepton+jets” topology, where one top quark decays semi-

leptonically ($t \rightarrow l\nu b$) and the other hadronically ($t \rightarrow q\bar{q}'b$) [17]. We detect the lepton and four jets from top quark decays and quark hadronization, and an inferred neutrino based on the presence of missing energy. The detector is triggered by a high transverse momentum lepton (electron or muon) in the central portion of the detector, or by $\cancel{E}_T > 35$ GeV if the event contains at least two energetic jets. This latter dataset makes up the “loose muon” sample, which is a new addition compared to the previous version of this analysis. We require that all candidate events contain exactly one electron or muon with $E_T(p_T) > 20$ GeV(GeV/c), as well as four or more hadronic jets with $E_T > 20$ GeV and $|\eta| < 2.0$. Jets are reconstructed using a cone algorithm with $\delta R = \sqrt{\delta\phi^2 + \delta\eta^2} < 0.4$, and calorimeter signals are corrected for detector inefficiencies with a jet energy scale factor. We require missing transverse energy, $\cancel{E}_T > 20$ GeV, consistent with the presence of an undetected neutrino. We finally require that H_T , the scalar sum of the transverse energy of all objects (lepton, jets, \cancel{E}_T) be $H_T > 220$ GeV, which leaves 97% of the signal but reduces the backgrounds by 17%. The SECVTX algorithm [18] is used to find displaced b -decay vertices using the tracks within the jet cones, and at least one jet must contain such a “ b -tag”. Jets with b -tags are restricted to $|\eta| < 1.0$.

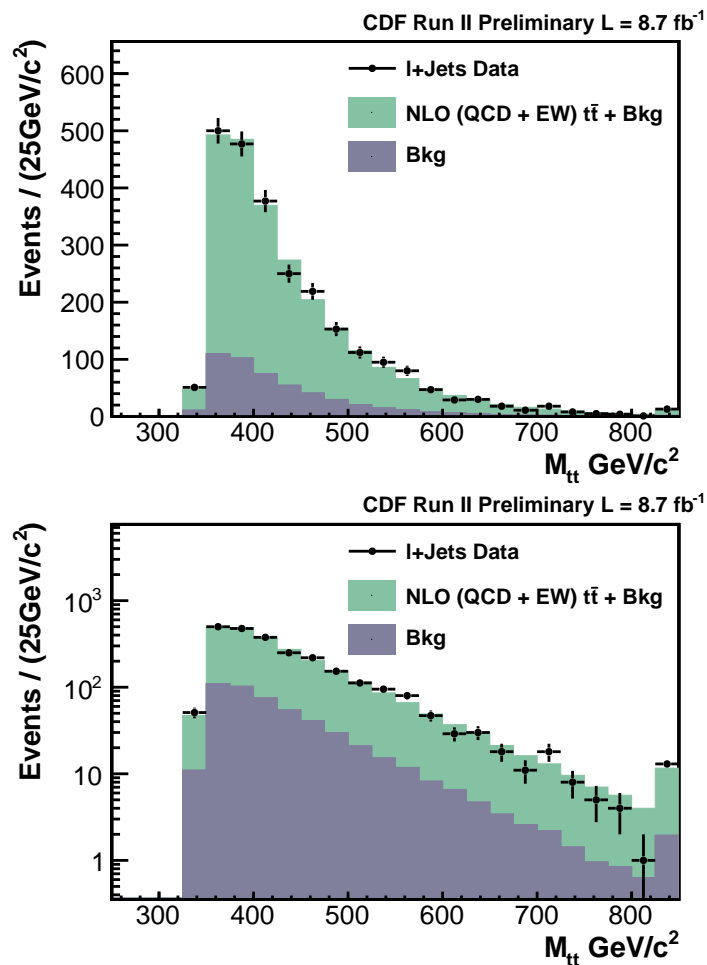


FIG. 1: Reconstructed mass of the $t\bar{t}$ system compared to the prediction of our background plus POWHEG model.

The sample passing this selection contains 2498 candidate events. The estimated non- $t\bar{t}$ background in our sample is 505 ± 123 events. The predominant backgrounds are from QCD-induced W +multi-parton events containing either b -tagged heavy-flavor jets or errantly tagged light-flavor jets. These are modeled with the ALPGEN generator [19] scaled by tagging efficiencies, mis-tagging rates, and sample normalizations from direct measurements. QCD multi-jet events with fake leptons and mis-measured \cancel{E}_T are modeled using multi-jet events with lepton candidates that are rejected by our cuts. Small backgrounds from electroweak processes (WW, WZ , single-top) are reliably estimated using Monte Carlo generators. The contributions from these various background sources are summarized

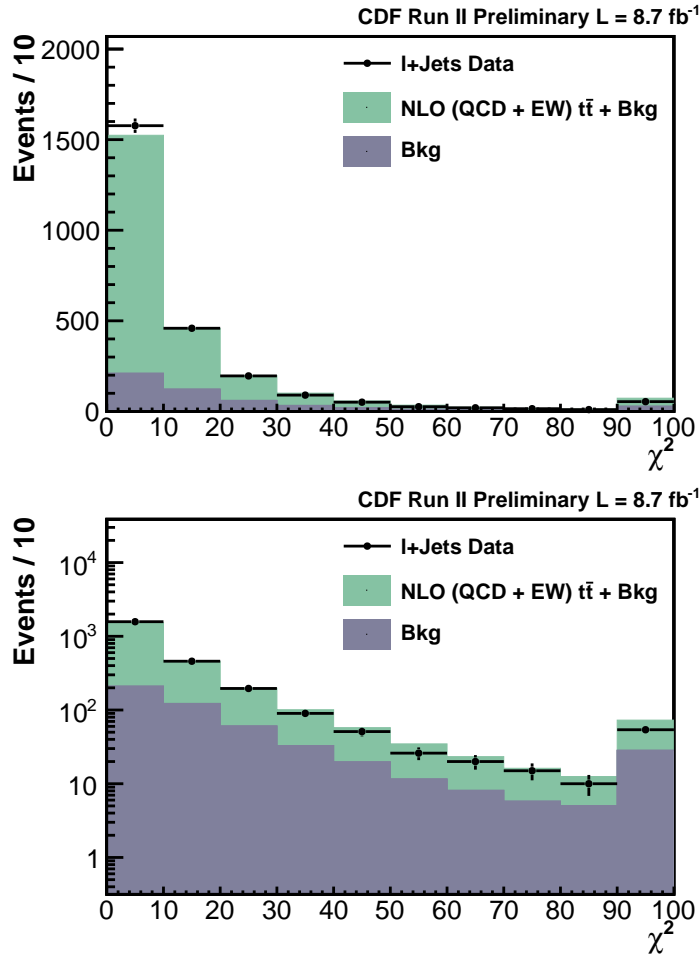


FIG. 2: χ^2 value for the kinematic fit.

in Table II.

The reconstruction of the $t\bar{t}$ kinematics employs the measured momenta of the lepton and the four leading jets in the event, along with the measured \cancel{E}_T . The jet-to-parton assignment and calculation of the $t\bar{t}$ four-vectors uses a simple χ^2 -based fit of the lepton and jet kinematics to the $t\bar{t}$ hypothesis, allowing the jet energies to float within their expected uncertainties, and applying the constraints that $M_W = 80.4 \text{ GeV}/c^2$, $M_t = 172.5 \text{ GeV}/c^2$, and b -tagged jets are associated with b -partons. The $t\bar{t}$ four-vectors determined in this manner specify the top quark rapidities and the Δy variable used for this analysis.

The validity of the analysis is checked at all steps by comparison to a standard prediction made using the POWHEG $t\bar{t}$ model, the CDF lepton+jets+ b -tag background model, and a full simulation of the CDF II detector. Figures 1 and 2 provide examples of the comparison of the data to our standard prediction in two important variables, the invariant mass of the $t\bar{t}$ system and the χ^2 value for the best kinematic fit of the event to the $t\bar{t}$ hypothesis.

The p_T of the $t\bar{t}$ system is a sensitive test of the reconstruction and modeling, particularly at low values, where both the prediction and the reconstruction are challenged by the presence of extra soft jets. Fig. 3 shows good agreement of the reconstructed data with the prediction from signal and background. With the background prediction subtracted, the NLO $t\bar{t}$ models are generally compatible with the data. There is less good agreement with PYTHIA (generated according to the standard CDF tune) or with a modified PYTHIA tune discussed in Ref. [5] that has no initial state radiation (ISR).

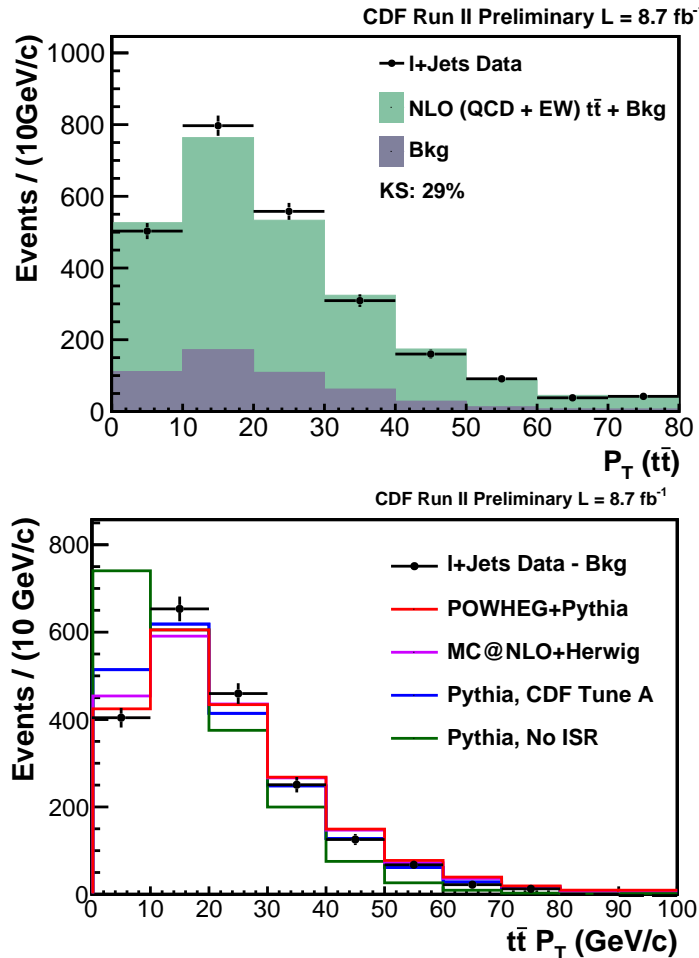


FIG. 3: Predicted p_T of the $t\bar{t}$ system and background. Background-subtracted data compared to several models.

IV. RAPIDITIES AND ASYMMETRIES IN THE RECONSTRUCTED DATA

The top direction is measured with frame-invariant difference of the t and \bar{t} rapidities, $\Delta y = y_t - y_{\bar{t}}$. In the limit where the p_T of the $t\bar{t}$ system is small, the asymmetry

$$A_{\text{FB}} = \frac{N(\Delta y > 0) - N(\Delta y < 0)}{N(\Delta y > 0) + N(\Delta y < 0)} \quad (1)$$

is identical to the asymmetry in the top quark production angle in the $t\bar{t}$ rest frame.

The reconstructed Δy distribution is shown for all the data in Fig. 4. The plot shows the measured asymmetry and the expected asymmetry for the NLO $t\bar{t}$ plus background prediction. Table III summarizes the asymmetry values in the inclusive sample and as a function of the lepton charge, and also compares with the 5.3 fb^{-1} results. The inclusive asymmetry in Δy is $A_{\text{FB}} = 0.066 \pm 0.020$ compared to 0.026 predicted. The uncertainties in the new analysis scale as expected from the previous analysis according to the increase in the number of candidate events. As before, when the sample is separated by lepton charge, the asymmetries are equal within errors, as expected from CP conservation.

We can make an additional check of our background estimates by considering the Δy distribution in events which pass all selection requirements except that they contain no b -tags. This sample is background-dominated, with only a small contribution from real $t\bar{t}$ events that do not contain a tagged jet. The Δy distribution in this sample is shown in Figure 5, and the observed asymmetry is in good agreement with the model prediction.

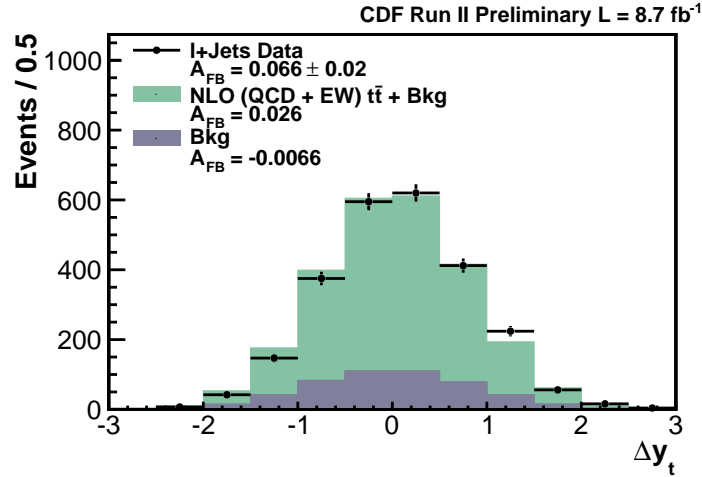


FIG. 4: The reconstructed Δy distribution.

CDF Run II Preliminary $L = 8.7 \text{ fb}^{-1}$		
	8.7 fb^{-1}	5.3 fb^{-1}
Selection	$A_{\text{FB}}(\pm\text{stat.})$	$A_{\text{FB}}(\pm\text{stat.})$
NLO (QCD+EW) $t\bar{t}$	0.033	
Backgrounds	-0.007	
Total Prediction	0.026	
All Data	0.066 ± 0.020	0.057 ± 0.028
Positive Leptons	0.077 ± 0.029	0.067 ± 0.040
Negative Leptons	0.056 ± 0.028	0.048 ± 0.039

TABLE III: Measured and expected asymmetries in Δy .

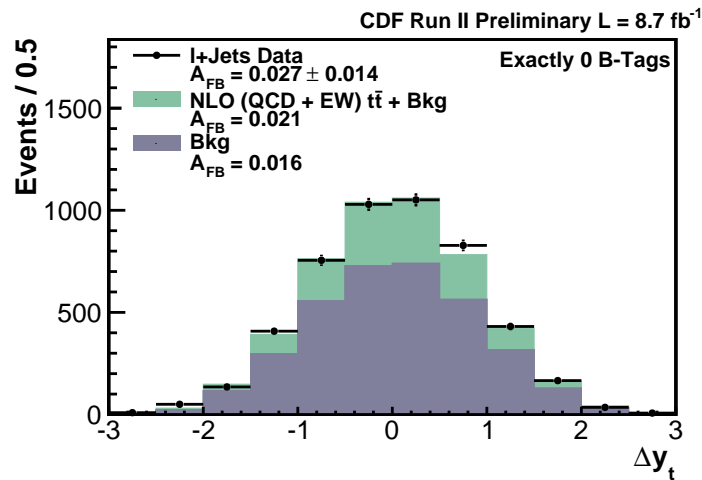


FIG. 5: Δy in the sample with no b -tagged jets.

A. Mass and Rapidity Dependence

The forward-backward asymmetry as a function of $|\Delta y|$ can be derived from the data in Fig. 4 using:

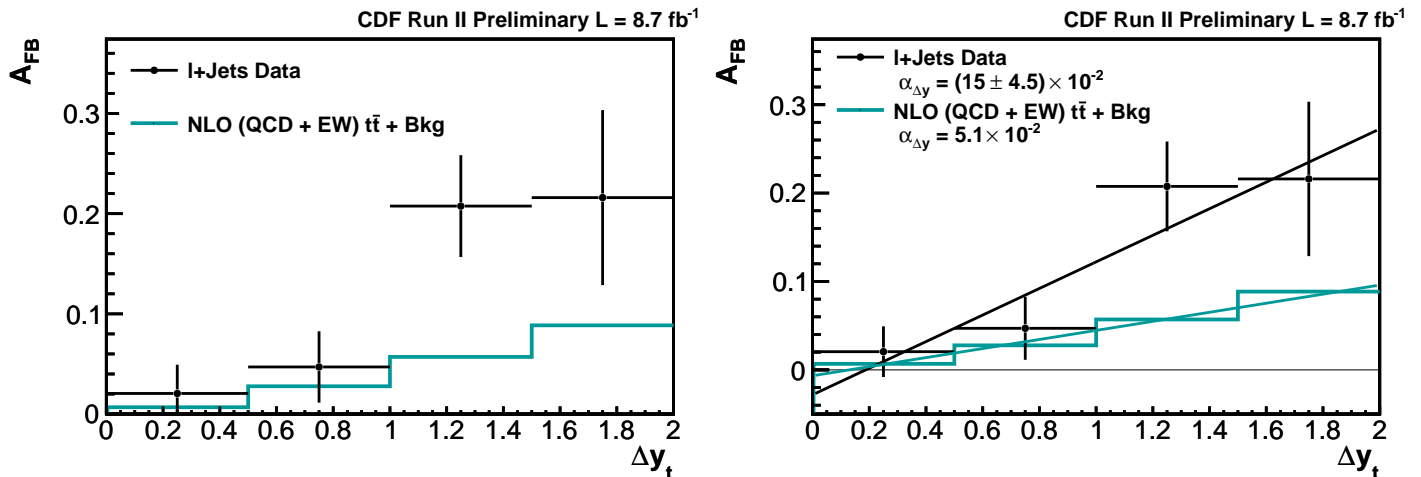


FIG. 6: A_{FB} as a function of $|\Delta y|$ (left) and the same distribution with a best-fit line superimposed (right).

$$A_{FB}(|\Delta y|) = \frac{N(\Delta y) - N(-\Delta y)}{N(\Delta y) + N(-\Delta y)} \quad (2)$$

$A_{FB}(|\Delta y|)$ is shown in four bins of Δy in Fig. 6 and Table IV. To quantify the function in a simple way, we assume a linear ansatz, which seems appropriate to the data and the POWHEG prediction. (See also Ref. [20]). The slope $\alpha_{\Delta y}$ of the line is not a parameter of any theory, but provides a simple way to compare the Δy behavior of the asymmetry in the data and prediction. The data is well fit by a line with χ^2 per degree of freedom $\chi_{pdf}^2 = 1.1$ and a slope $\alpha_{\Delta y} = (15.0 \pm 4.5) \times 10^{-2}$, compared to a prediction of 5.1×10^{-2} .

CDF Run II Preliminary L = 8.7 fb ⁻¹			
	Data	NLO (QCD+EW) $t\bar{t}$ + Bkg.	
$ \Delta y $	$A_{FB} (\pm \text{stat.})$	A_{FB}	
0.0 - 0.5	0.021 ± 0.029	0.007	
0.5 - 1.0	0.047 ± 0.036	0.028	
1.0 - 1.5	0.208 ± 0.051	0.057	
≥ 1.5	0.216 ± 0.087	0.089	
	Data	NLO (QCD+EW) $t\bar{t}$ + Bkg.	
Slope $\alpha_{\Delta y}$ of Linear Fit	$(15.0 \pm 4.5) \times 10^{-2}$	5.1×10^{-2}	

TABLE IV: Measured and expected asymmetries as a function of $|\Delta y|$.

We also consider the behavior of the asymmetry with the invariant mass of the $t\bar{t}$ system, $M_{t\bar{t}}$. Dividing into several mass bins and determining the number of events with positive (N_F) and negative (N_B) Δy in each bin, we find the forward-backward asymmetry as a function of $M_{t\bar{t}}$ as:

$$A_{FB}(M_{t\bar{t}}) = \frac{N_F(M_{t\bar{t}}) - N_B(M_{t\bar{t}})}{N_F(M_{t\bar{t}}) + N_B(M_{t\bar{t}})} \quad (3)$$

The $M_{t\bar{t}}$ dependent asymmetry is compared to the NLO prediction in Fig. 7 and Table V. These are bins of 50 GeV/c² below 600 GeV/c², then a 100 GeV/c² bin, then an overflow bin. The data and prediction are again approximately linear, and we find the best fit line as before. The data is described by a line with $\chi_{pdf}^2 = 0.25$ and a slope $\alpha_{M_{t\bar{t}}} = (8.9 \pm 2.3) \times 10^{-4}$ compared to a prediction of 2.2×10^{-4} . Figure 8 and Table VI show the same data and fit in the four bin choice that will later be used in deriving our parton level results.

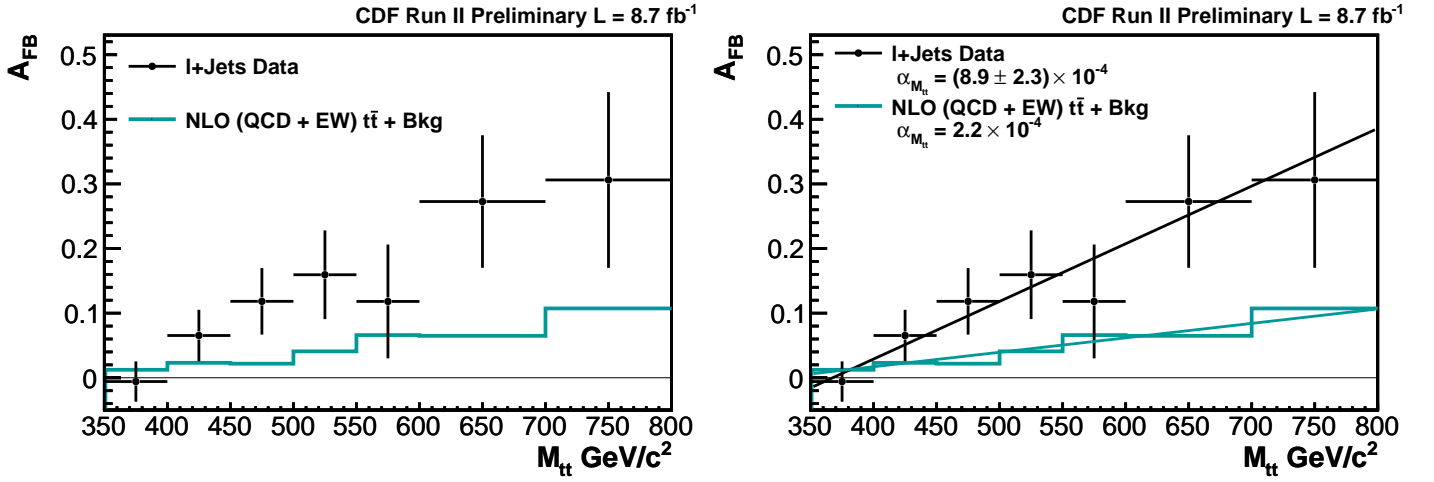


FIG. 7: A_{FB} as a function of $M_{t\bar{t}}$ (left) and the same distribution with a best-fit line superimposed (right).

CDF Run II Preliminary L = 8.7 fb ⁻¹		
$M_{t\bar{t}}$	Data $A_{FB} (\pm \text{stat.})$	NLO (QCD+EW) $t\bar{t}$ + Bkg. A_{FB}
$< 400 \text{ GeV}/c^2$	-0.006 ± 0.031	0.012
$400 - 450 \text{ GeV}/c^2$	0.065 ± 0.040	0.023
$450 - 500 \text{ GeV}/c^2$	0.118 ± 0.051	0.022
$500 - 550 \text{ GeV}/c^2$	0.159 ± 0.069	0.041
$550 - 600 \text{ GeV}/c^2$	0.118 ± 0.088	0.066
$600 - 700 \text{ GeV}/c^2$	0.273 ± 0.103	0.065
$\geq 700 \text{ GeV}/c^2$	0.306 ± 0.136	0.107
Data NLO (QCD+EW) $t\bar{t}$ + Bkg.		
Slope $\alpha_{M_{t\bar{t}}}$ of Best-Fit Line $(8.9 \pm 2.3) \times 10^{-4}$ 2.2×10^{-4}		

TABLE V: Measured and expected asymmetries as a function of $M_{t\bar{t}}$.

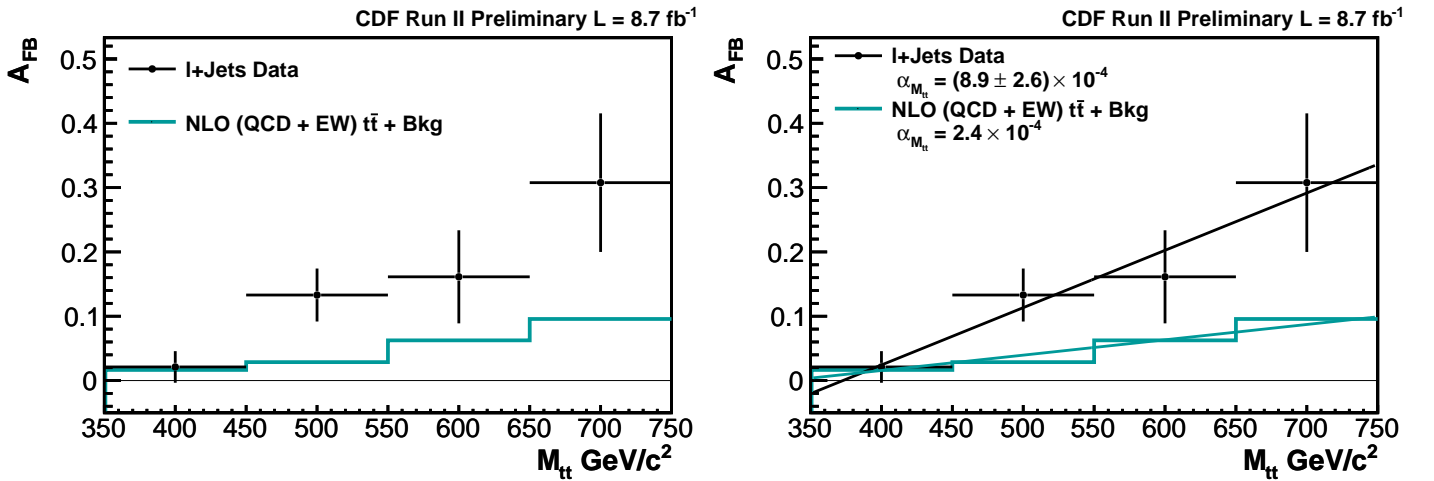
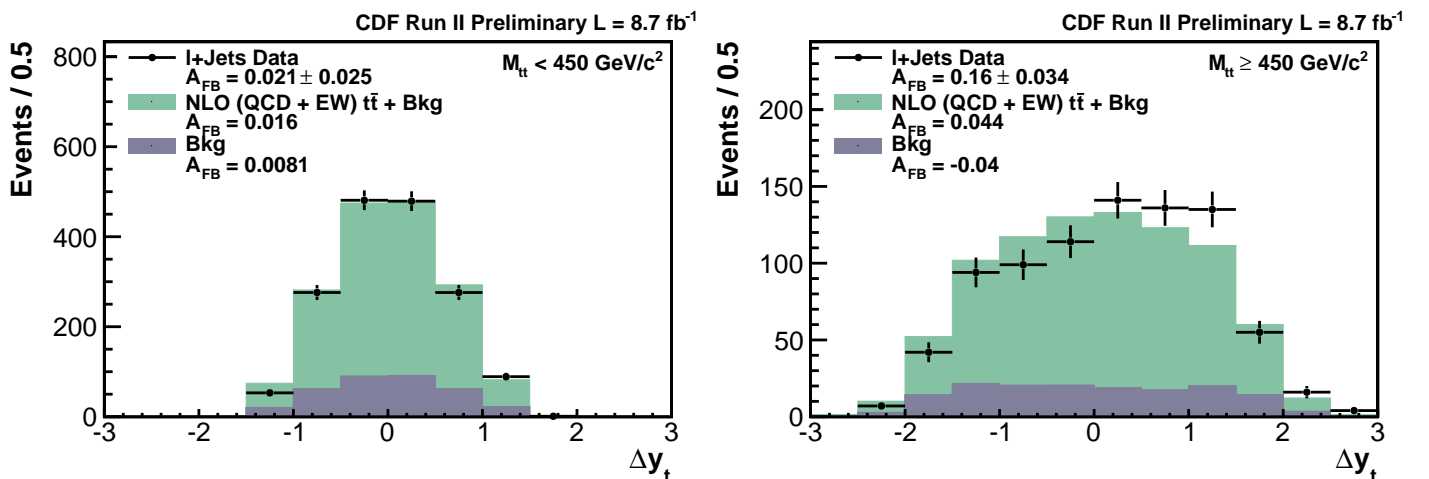


FIG. 8: Alternative binning of A_{FB} as a function of $M_{t\bar{t}}$ (left) and the same distribution with a best-fit line superimposed (right).

CDF Run II Preliminary L = 8.7 fb ⁻¹		
$M_{t\bar{t}}$	Data	NLO (QCD+EW) $t\bar{t}$ + Bkg.
	$A_{\text{FB}} (\pm \text{stat.})$	A_{FB}
$< 450 \text{ GeV}/c^2$	0.021 ± 0.025	0.017
$450 - 550 \text{ GeV}/c^2$	0.133 ± 0.041	0.029
$550 - 650 \text{ GeV}/c^2$	0.161 ± 0.072	0.063
$\geq 650 \text{ GeV}/c^2$	0.308 ± 0.108	0.096
Slope $\alpha_{M_{t\bar{t}}}$ of Best-Fit Line		
	$(8.9 \pm 2.6) \times 10^{-4}$	2.4×10^{-4}

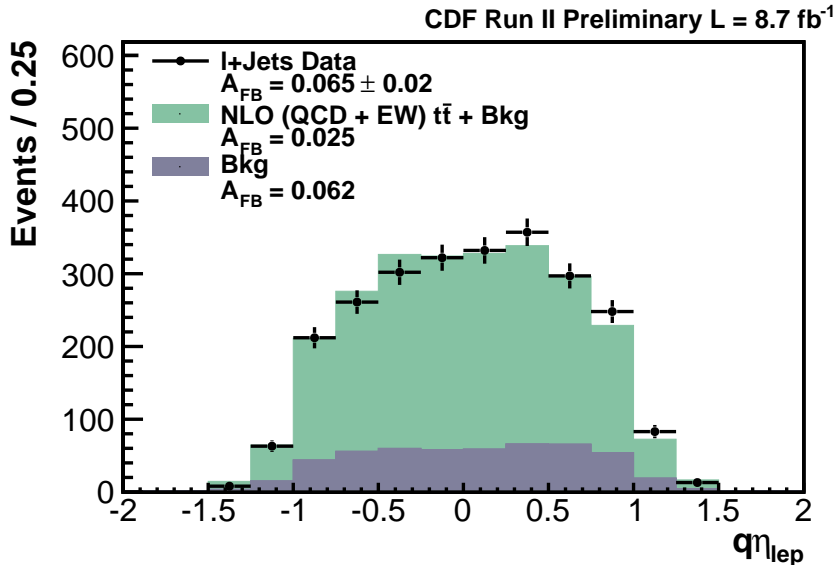
TABLE VI: Measured and expected asymmetries as a function of $M_{t\bar{t}}$ with alternative binning.

As was done in the 5.3 fb⁻¹ analysis, we consider the partition of the data into two bins of mass, above and below 450 GeV/c². The Δy distributions at high and low mass, shown in Fig. 9, show the same growth of A_{FB} as in the earlier result, although the difference between the two cases is somewhat moderated in the full dataset. The asymmetry is 0.021 ± 0.025 for $M_{t\bar{t}} < 450 \text{ GeV}/c^2$ and 0.155 ± 0.034 for $M_{t\bar{t}} \geq 450 \text{ GeV}/c^2$. The behavior of the asymmetry at high and low $M_{t\bar{t}}$ in various subsets of our data is summarized in Table VII. The $M_{t\bar{t}}$ dependence is consistent across lepton charge and lepton type. It is small in events without b -tags (as expected in this background-dominated sample), and it is consistent (within relatively large statistical uncertainty) across single and double tags.

FIG. 9: Reconstructed Δy for events with $M_{t\bar{t}} < 450 \text{ GeV}/c^2$ (left) and $M_{t\bar{t}} \geq 450 \text{ GeV}/c^2$ (right).

CDF Run II Preliminary L = 8.7 fb ⁻¹			
Sample	$A_{\text{FB}} (\pm \text{stat.})$ Inclusive	$A_{\text{FB}} (\pm \text{stat.})$ $M_{t\bar{t}} < 450 \text{ GeV}/c^2$	$A_{\text{FB}} (\pm \text{stat.})$ $M_{t\bar{t}} \geq 450 \text{ GeV}/c^2$
All Data	0.066 ± 0.020	0.021 ± 0.025	0.155 ± 0.034
Positive Leptons	0.077 ± 0.029	0.036 ± 0.036	0.155 ± 0.048
Negative Leptons	0.056 ± 0.028	0.008 ± 0.034	0.156 ± 0.048
Exactly 0 b -tags	0.027 ± 0.014	0.036 ± 0.017	0.005 ± 0.026
Exactly 1 b -tags	0.078 ± 0.023	0.031 ± 0.028	0.172 ± 0.039
At Least 2 b -tags	0.028 ± 0.042	-0.014 ± 0.052	0.103 ± 0.070
Electron Events	0.044 ± 0.030	-0.012 ± 0.036	0.155 ± 0.050
Muon Events	0.085 ± 0.027	0.049 ± 0.033	0.155 ± 0.046

TABLE VII: Measured asymmetries in various subsets of the data.

FIG. 10: Reconstructed $q \cdot \eta_{lep}$.

B. The Lepton Asymmetry

The direction of motion of the lepton from a semi-leptonic top decay is correlated with the direction of motion of the parent top quark. Thus, if a $t\bar{t}$ production asymmetry exists, it should also be observable as an asymmetry in the direction of motion of the decay lepton. We look for such an asymmetry in the observable $q \cdot \eta_{lep}$, shown in Figure 10, finding an asymmetry of 0.065 ± 0.020 . The asymmetry in this variable for $M_{t\bar{t}}$ above and below $450 \text{ GeV}/c^2$ is shown in Table VIII and compared to the model prediction.

CDF Run II Preliminary L = 8.7 fb ⁻¹		
	Data	NLO (QCD+EW) $t\bar{t}$ + Bkg.
$M_{t\bar{t}}$	$A_{FB} (\pm \text{stat.})$	A_{FB}
Inclusive	0.065 ± 0.020	0.025
$< 450 \text{ GeV}/c^2$	0.047 ± 0.025	0.023
$\geq 450 \text{ GeV}/c^2$	0.101 ± 0.034	0.033

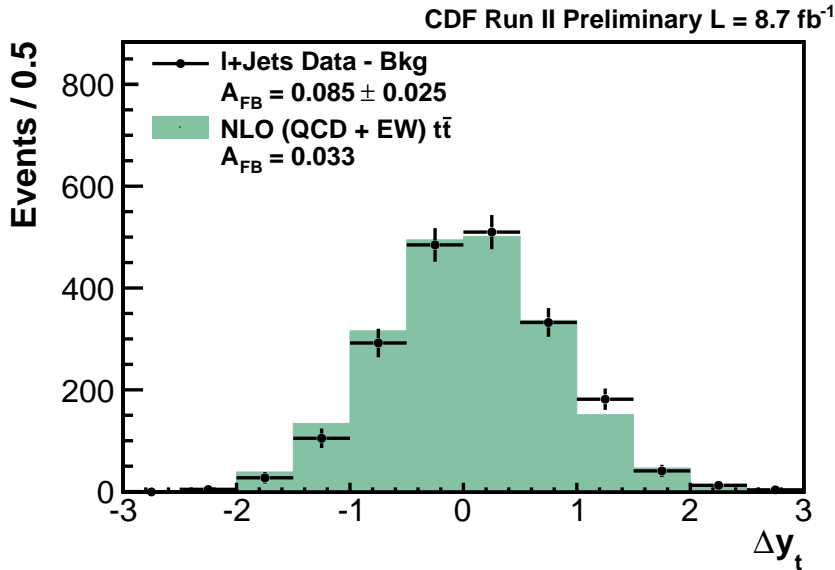
TABLE VIII: Measured and expected asymmetries in $q \cdot \eta_{lep}$.

V. ASYMMETRIES AFTER BACKGROUND SUBTRACTION

At this stage, approximately 20% of the analyzed data is composed of events originating from various background sources. We now want to remove these background contributions in order to focus on the asymmetry in the $t\bar{t}$ events themselves. In order to do so, we subtract the predicted background contribution from our observed distributions. Because there is some uncertainty in the predicted backgrounds, this background subtraction procedure introduces a systematic uncertainty, which is added to our statistical uncertainty as in Equation 4.

$$\sigma_{tot}^2 = \sigma_{stat}^2 + \sigma_{syst,bkg.norm}^2 + \sigma_{syst,bkg.MCstat}^2 + \sigma_{syst,bkg.shape}^2 \quad (4)$$

Here, σ_{stat} is the statistical uncertainty on our observed data in each bin. $\sigma_{syst,bkg.norm}$ is a contribution due to the uncertainty in the predictions for the background normalizations, based on the values in Table II, and

FIG. 11: Background subtracted Δy .

$\sigma_{syst,bkg.MCstat}$ is a contribution from the uncertainty on the shape of each background component due to the statistics of the sample used to model that component. $\sigma_{syst,bkg.shape}$ describes an overall shape uncertainty on the background estimated by comparing our observed data in events with no b -tags to the prediction for that background-dominated sample. In total, the sum of the systematic contributions to the uncertainty is generally less than 20% of the statistical uncertainty on a given quantity. All distributions and results in this section include both statistical and systematic uncertainties.

The Δy distribution after background subtraction is given in Figure 11. Although the total background prediction has a small asymmetry, the removal of this background decreases the dilution of the $t\bar{t}$ signal asymmetry, resulting in an increase in the observed asymmetry in the background subtracted sample to 0.085 ± 0.025 , compared to the POWHEG prediction of 0.033.

A. The Asymmetry Over the Run II Data-Taking Period

To investigate whether the asymmetry could result from some run-dependent mis-calibration or other temporary issue over the course of the long CDF Run II data-taking period, we study its behavior over time as the number of candidate $t\bar{t}$ events increases. Figure 12 shows the measured asymmetry after background subtraction and its uncertainty as a function of the total number of events in our $t\bar{t}$ signal sample, with 0 events corresponding to the beginning of Run II. As expected from a real asymmetry, the observed A_{FB} remains constant within uncertainties, with the significance increasing with the sample size.

B. Mass and Rapidity Dependence

$A_{FB}(|\Delta y|)$ for the background-free reconstructed $t\bar{t}$ signal is shown in Figure 13 and Table IX. The data and prediction are again well fit by the linear assumption, with an observed slope of $\alpha_{\Delta y} = (20.0 \pm 5.9) \times 10^{-2}$ compared to the predicted 6.7×10^{-2} .

We also consider the $M_{t\bar{t}}$ dependence of the background subtracted asymmetry. Figure 14 compares the $M_{t\bar{t}}$ distributions in the observed forward and backward events. We can convert these distributions into asymmetries as a function of $M_{t\bar{t}}$, shown in Figure 15 and summarized in Table X, along with the best-fit slope $\alpha_{M_{t\bar{t}}}$. The linear assumption has $\chi^2_{pdf} = 0.34$. The $A_{FB}(M_{t\bar{t}})$ distribution, along with the measured asymmetries and slope, based on the same binning that will be used for our parton level results is given in Figure 8 and Table XI.

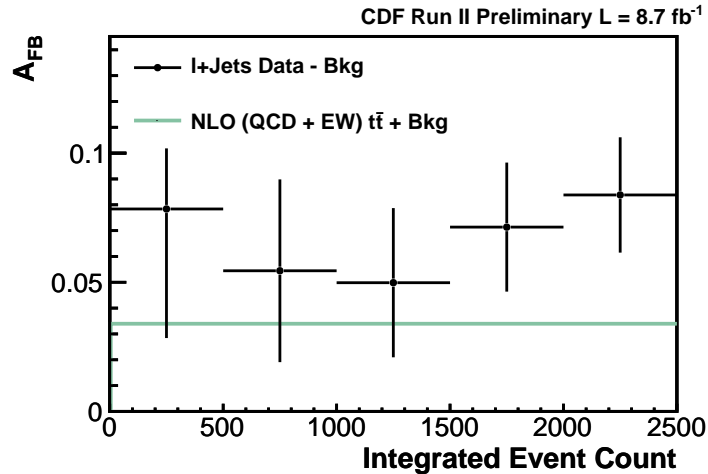


FIG. 12: Background subtracted A_{FB} as a function of the number of observed events in the CDF Run II dataset.

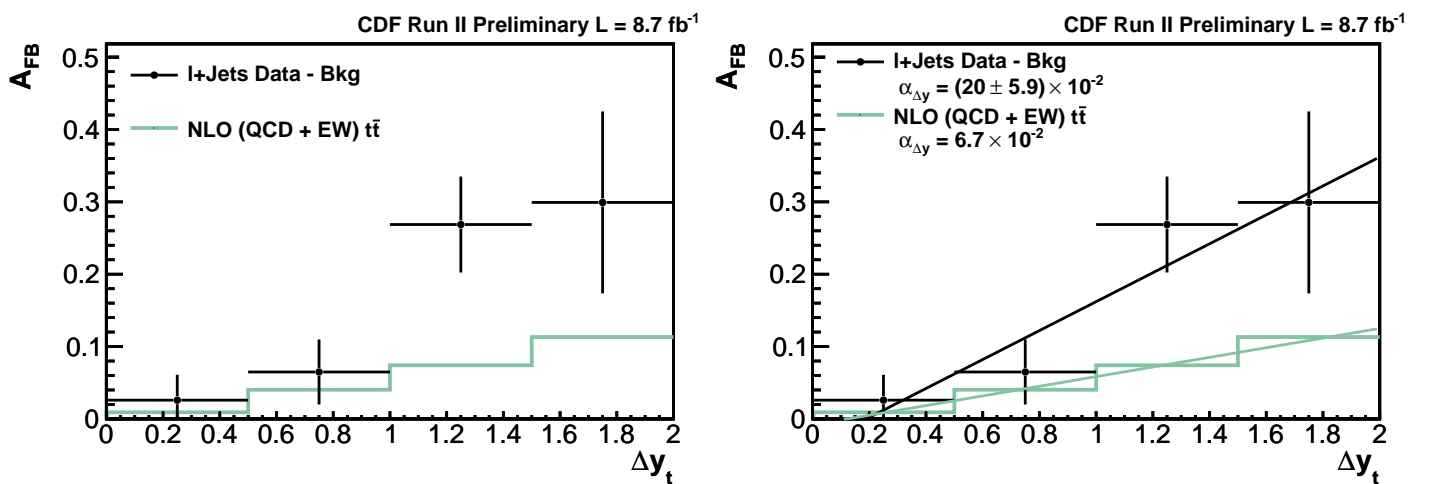


FIG. 13: Background subtracted A_{FB} as a function of $|\Delta y|$ (left) and the same distribution with a best-fit line superimposed (right).

CDF Run II Preliminary L = 8.7 fb ⁻¹		
	Data	NLO (QCD+EW) $t\bar{t}$
$ \Delta y $	$A_{FB} (\pm [\text{stat.}+\text{syst.}])$	A_{FB}
0.0 - 0.5	0.026 ± 0.035	0.009
0.5 - 1.0	0.065 ± 0.045	0.040
1.0 - 1.5	0.269 ± 0.066	0.074
≥ 1.5	0.299 ± 0.126	0.113
	Data	NLO (QCD+EW) $t\bar{t}$
Slope $\alpha_{\Delta y}$ of Best-Fit Line	$(20.0 \pm 5.9) \times 10^{-2}$	6.7×10^{-2}

TABLE IX: Measured and expected asymmetries as a function of $|\Delta y|$ after background subtraction.

At the background subtracted level, we again consider the partition of the data into two bins of $M_{t\bar{t}}$. The Δy distributions at high and low mass are shown in Fig. 17, yielding asymmetries of 0.025 ± 0.031 for $M_{t\bar{t}} < 450 \text{ GeV}/c^2$ and 0.198 ± 0.043 for $M_{t\bar{t}} \geq 450 \text{ GeV}/c^2$. The behavior of the background subtracted asymmetry at high and low

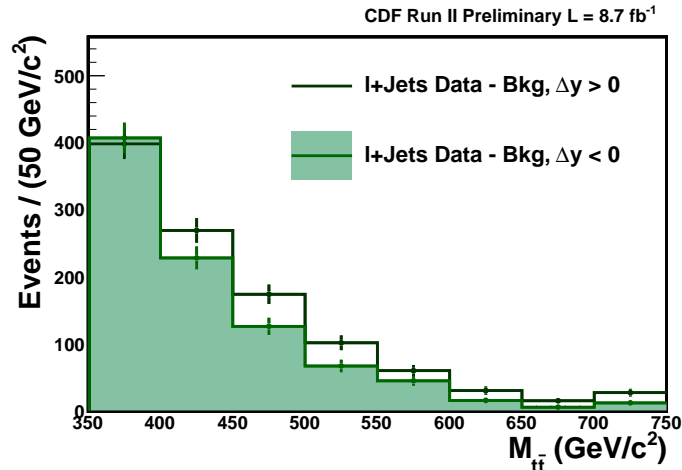


FIG. 14: $M_{t\bar{t}}$ after background subtraction in events with positive and negative Δy .

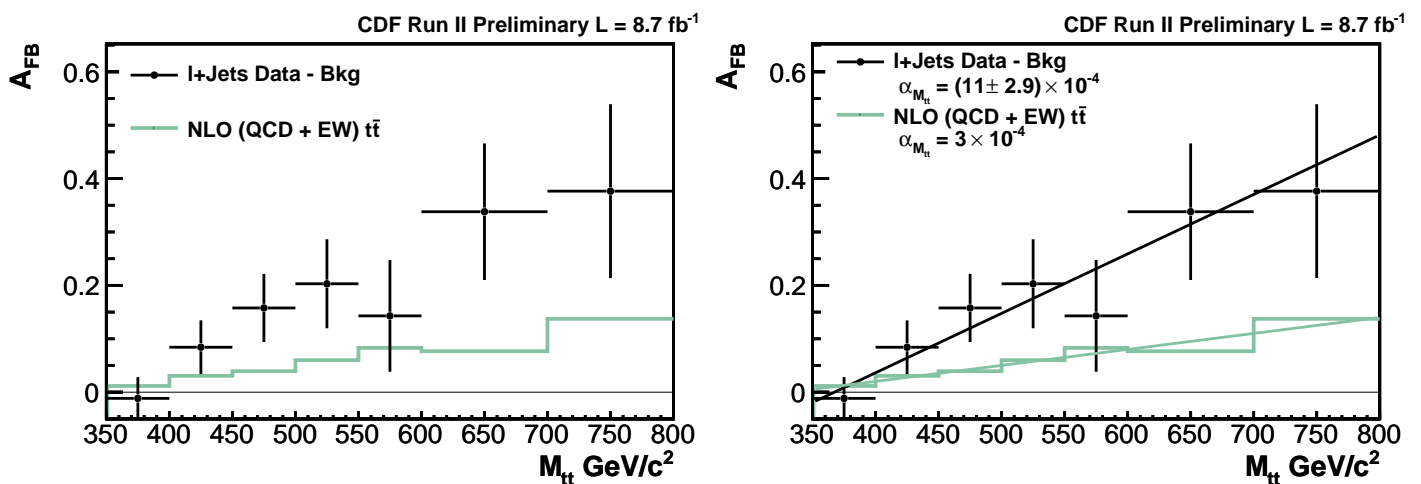


FIG. 15: Background subtracted A_{FB} as a function of $M_{t\bar{t}}$ (left) and the same distribution with a best-fit line superimposed (right).

CDF Run II Preliminary L = 8.7 fb ⁻¹		
$M_{t\bar{t}}$	Data $A_{\text{FB}} (\pm [\text{stat.}+\text{syst.}])$	NLO (QCD+EW) $t\bar{t}$ A_{FB}
$< 400\text{GeV}/c^2$	-0.012 ± 0.040	0.012
$400 - 450\text{GeV}/c^2$	0.084 ± 0.050	0.031
$450 - 500\text{GeV}/c^2$	0.158 ± 0.064	0.039
$500 - 550\text{GeV}/c^2$	0.203 ± 0.083	0.060
$550 - 600\text{GeV}/c^2$	0.143 ± 0.105	0.083
$600 - 700\text{GeV}/c^2$	0.338 ± 0.128	0.077
$\geq 700\text{GeV}/c^2$	0.377 ± 0.163	0.137
Data NLO (QCD+EW) $t\bar{t}$		
Slope $\alpha_{M_{t\bar{t}}}$ of Best-Fit Line	$(11.1 \pm 2.9) \times 10^{-4}$	3.0×10^{-4}

TABLE X: Measured and expected asymmetries as a function of $M_{t\bar{t}}$ after background subtraction.

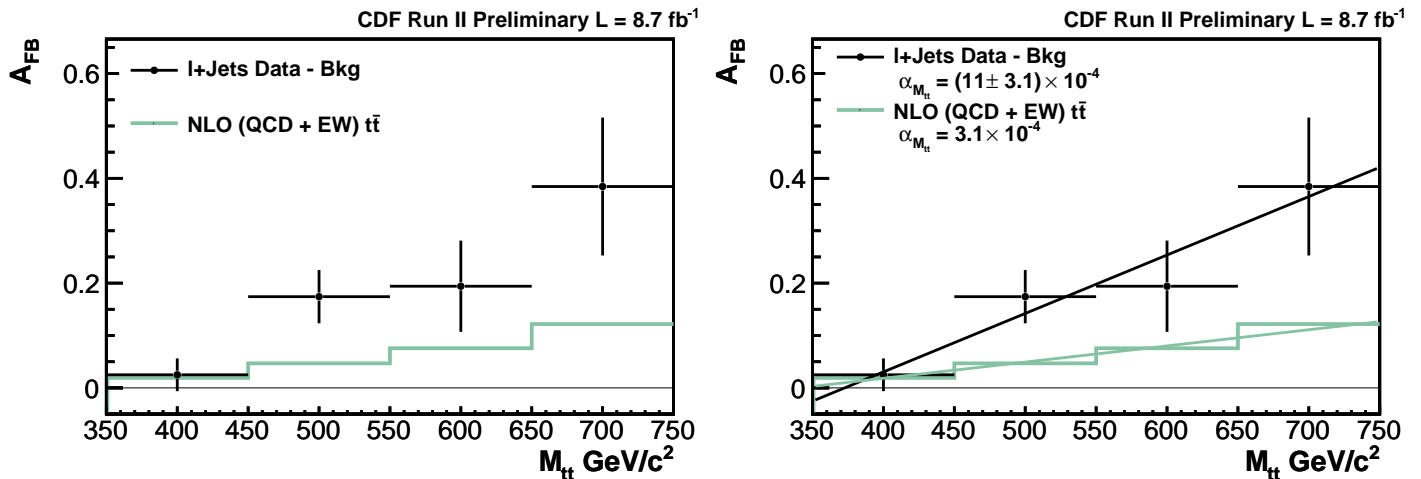


FIG. 16: Background subtracted A_{FB} as a function of $M_{t\bar{t}}$ (left) and the same distribution with a best-fit line superimposed (right) with an alternate binning of $M_{t\bar{t}}$.

CDF Run II Preliminary L = 8.7 fb ⁻¹		
$M_{t\bar{t}}$	Data $A_{FB} (\pm [\text{stat.}+\text{syst.}])$	NLO (QCD+EW) $t\bar{t}$ A_{FB}
$< 450\text{GeV}/c^2$	0.025 ± 0.031	0.019
$450 - 550\text{GeV}/c^2$	0.174 ± 0.051	0.047
$550 - 650\text{GeV}/c^2$	0.194 ± 0.087	0.076
$\geq 650\text{GeV}/c^2$	0.384 ± 0.132	0.122
Slope $\alpha_{M_{t\bar{t}}}$ of Best-Fit Line		
	Data $(11.2 \pm 3.1) \times 10^{-4}$	NLO (QCD+EW) $t\bar{t}$ 3.1×10^{-4}

TABLE XI: Measured and expected asymmetries after background subtraction as a function of $M_{t\bar{t}}$ with an alternate binning.

$M_{t\bar{t}}$ in various subsets of our data is summarized in Table XII. As seen in the full sample before background subtraction, the $M_{t\bar{t}}$ dependence is consistent across lepton charge and lepton type. It is again consistent (within relatively large statistical uncertainty) across single and double tags.

CDF Run II Preliminary L = 8.7 fb ⁻¹			
Sample	$A_{FB} (\pm [\text{stat.}+\text{syst.}])$ Inclusive	$A_{FB} (\pm [\text{stat.}+\text{syst.}])$ $M_{t\bar{t}} < 450\text{GeV}/c^2$	$A_{FB} (\pm [\text{stat.}+\text{syst.}])$ $M_{t\bar{t}} \geq 450\text{GeV}/c^2$
All Data	0.085 ± 0.025	0.025 ± 0.031	0.198 ± 0.043
Positive Leptons	0.100 ± 0.037	0.044 ± 0.046	0.198 ± 0.060
Negative Leptons	0.071 ± 0.035	0.008 ± 0.043	0.198 ± 0.059
Exactly 0 b -tags	0.056 ± 0.052	0.079 ± 0.066	0.005 ± 0.085
Exactly 1 b -tags	0.103 ± 0.030	0.039 ± 0.037	0.226 ± 0.050
At least 2 b -tags	0.034 ± 0.046	-0.014 ± 0.057	0.122 ± 0.077
Electron Events	0.058 ± 0.038	-0.018 ± 0.048	0.199 ± 0.062
Muon Events	0.107 ± 0.034	0.060 ± 0.041	0.197 ± 0.057

TABLE XII: Measured asymmetries after background subtraction in various subsets of the data.

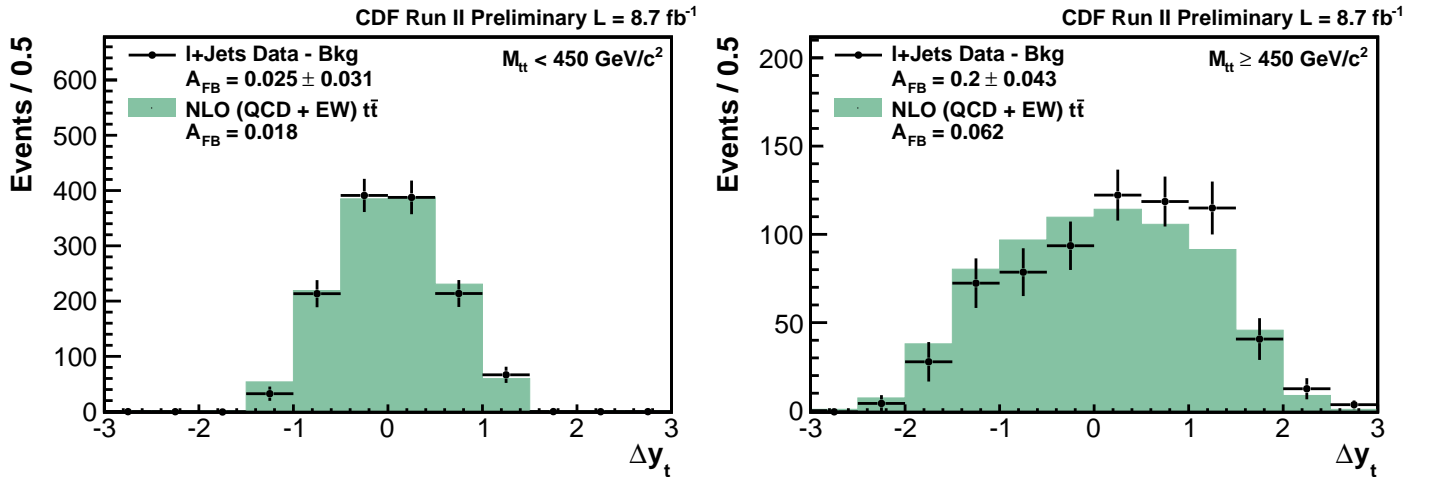


FIG. 17: Δy after background subtraction for events with $M_{t\bar{t}} < 450 \text{ GeV}/c^2$ (left) and $M_{t\bar{t}} \geq 450 \text{ GeV}/c^2$ (right).

C. Transverse Momentum Dependence

As in mass and rapidity, we study the dependance of the asymmetry on the p_T of the $t\bar{t}$ system by determining the number of events with positive or negative Δy in each of several bins, and defining the per-bin asymmetry as

$$A_{\text{FB}}(p_T) = \frac{N_F(p_T) - N_B(p_T)}{N_F(p_T) + N_B(p_T)} \quad (5)$$

Fig. 18 and Tab. XIII show this dependence in bins of $10 \text{ GeV}/c$, one-half of our p_T resolution. Also shown are two predictions: the NLO POWHEG model which serves as our standard prediction, and the LO PYTHIA model, which despite lacking an inclusive A_{FB} nevertheless shows a strong p_T dependent asymmetry which is different from POWHEG. Like both models, the data A_{FB} decreases with increasing p_T .

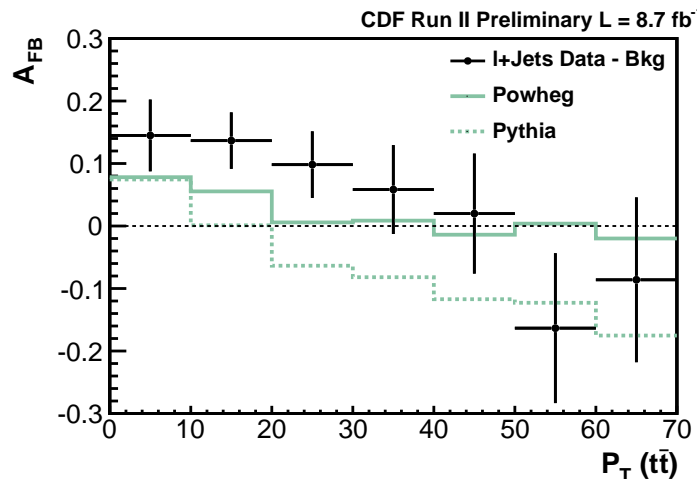


FIG. 18: A_{FB} as a function of the p_T of the $t\bar{t}$ system.

CDF Run II Preliminary L = 8.7 fb ⁻¹			
$p_T(\text{GeV}/c)$	Signal Level	POWHEG	Pythia
0 – 10	0.145 ± 0.057	0.078	0.074
10 – 20	0.137 ± 0.045	0.055	0.001
20 – 30	0.098 ± 0.053	0.006	-0.064
30 – 40	0.058 ± 0.071	0.009	-0.082
40 – 50	0.020 ± 0.096	-0.014	-0.117
50 – 60	-0.163 ± 0.120	0.004	-0.123
≥ 60	-0.086 ± 0.132	-0.020	-0.175

TABLE XIII: Measured asymmetry as a function of p_T after background subtraction.

D. Determination of the Significance

We determine the significance of the observed $|\Delta y|$ and $M_{t\bar{t}}$ dependence of the asymmetry at the background subtracted level by comparing the observed slopes $\alpha_{\Delta y, M_{t\bar{t}}}$ to the POWHEG prediction. To do this, we perform simulated experiments to determine how often we should expect a statistical fluctuation of POWHEG to result in a slope as large as that observed in the data. Starting with the prediction of POWHEG plus the various background sources, we fluctuate the contribution from the $t\bar{t}$ signal and each background source. For each simulated experiment, the nominal background prediction is subtracted, and the slope of the remaining background-subtracted differential asymmetry is measured. The p-value is determined to be the fraction of simulated experiments in which the slope exceeds that which we observe in our data. We find a p-value of 0.00892 for $A_{\text{FB}}(|\Delta y|)$ and 0.00646 for $A_{\text{FB}}(M_{t\bar{t}})$ (based on the 4-bin version of the $M_{t\bar{t}}$ distribution), as shown in Table XIV.

CDF Run II Preliminary L = 8.7 fb ⁻¹	
Slope Parameter	Data p-value
$\alpha_{\Delta y} (A_{\text{FB}} \text{ vs. } \Delta y)$	0.00892
$\alpha_{M_{t\bar{t}}} (A_{\text{FB}} \text{ vs. } M_{t\bar{t}})$	0.00646

TABLE XIV: The significance of the slopes $\alpha_{\Delta y, M_{t\bar{t}}}$ of the background subtracted differential asymmetries.

E. The Background-Subtracted Lepton Asymmetry

We can also consider the asymmetry in the lepton direction of motion after background subtraction. In this case, the asymmetry in the background prediction is large (of the same order as the observed asymmetry) because of a large contribution from standard model W boson production. The observed $q \cdot \eta_{lep}$ distribution after background subtraction is shown in Figure 19 and yields an asymmetry of 0.066 ± 0.025 . The behavior of this asymmetry with $M_{t\bar{t}}$ is given in Table XV.

CDF Run II Preliminary L = 8.7 fb ⁻¹		
$M_{t\bar{t}}$	Data	NLO (QCD+EW) $t\bar{t}$
	$A_{\text{FB}} (\pm [\text{stat.}+\text{syst.}])$	A_{FB}
Inclusive	0.066 ± 0.025	0.016
$< 450\text{GeV}/c^2$	0.037 ± 0.031	0.007
$\geq 450\text{GeV}/c^2$	0.116 ± 0.042	0.032

TABLE XV: Measured and expected asymmetries in $q \cdot \eta_{lep}$ after background subtraction

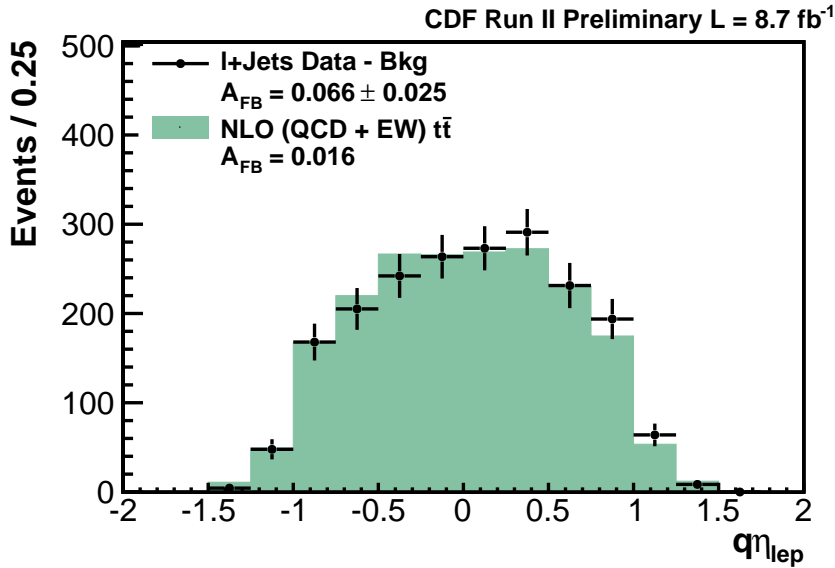


FIG. 19: $q \cdot \eta_{lep}$ after background subtraction.

VI. CORRECTION TO THE PARTON LEVEL

The background-subtracted results of the previous section provide a measurement of the asymmetry in a sample composed purely of $t\bar{t}$ events. However, these results are not directly comparable to theoretical predictions because the measured results also include effects introduced by our limited acceptance and by the resolution of the detector. We now correct for these effects in order to provide parton level results that can be directly compared to theory predictions.

The correction procedure takes place in two distinct steps. We first correct for the resolution of our detector, which results in the measured value of Δy not necessarily corresponding to the true Δy in a given event. This effect is accounted for using a regularized unfolding algorithm based on Singular Value Decomposition (SVD) [21]. In particular, we use the version of this algorithm implemented in the ROOUNFOLD software package [22]. We model the bin-to-bin migration caused by our detector using POWHEG, and then invert this response matrix and apply it to the data, in conjunction with a regularization term that prevents small statistical fluctuations from dominating the correction procedure.

Second, we correct for our limited acceptance, which results in us not being able to detect all $t\bar{t}$ events that are produced in the collisions that take place within CDF. We correct for this effect with a simple diagonal matrix - a multiplicative correction to each bin of Δy corresponding to the acceptance in that bin, as derived using the POWHEG model.

The combination of these two parts of the correction procedure allows us to determine the parton level distribution of Δy , which we report as a differential cross-section. This algorithm was tested in various simulated $t\bar{t}$ samples, including standard model POWHEG and the non-standard model samples Octet A and Octet B. Analyzing these samples as if they were data, we measured the bias in the comparison of derived “parton-level” results to the true values in the generated samples. The POWHEG results were self-consistent to $< 1\%$, and, with the NLO standard model as our assumption, any biases observed in this case are included as systematic uncertainties. In the Octet models, the derived distributions tracked the generator truth predictions well, but small biases (generally $\lesssim 2 - 4\%$) were observed in some of the differential asymmetry values. Since we have no reason to believe these models represent the real physics, we do not attempt to correct these biases or include them in the uncertainty. But in light of this model-dependence, we emphasize that our parton-level results need to be interpreted with some caution in relation to models that differ significantly from the NLO standard model. This is why the p-value to the standard model was derived with the detector-level data only.

Because the resolution corrections migrate events from bin to bin, the bins in the final parton level distributions are correlated. In all binned parton level distributions shown here, the uncertainties are per bin, but they are not independent. When we calculate quantities like the slopes of lines through the binned data we have used the

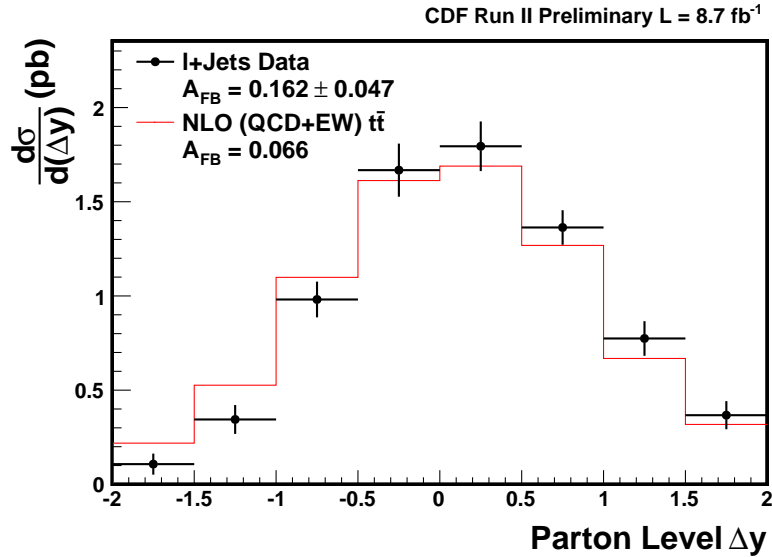


FIG. 20: Differential cross-section $d\sigma/d(\Delta y)$.

covariance matrix created during the unsmearing procedure to properly propagate the errors.

Several source of systematic uncertainty must be accounted for when applying the correction procedure. In addition to uncertainties on the size and shape of the background prediction, as discussed previously for the background subtracted results, there are also uncertainties on the signal Monte Carlo sample used to model our acceptance and detector response, including the size of the jet energy scale corrections, the amount of initial and final state radiation, the models used for color reconnection and parton showering, and the underlying parton distribution functions. We also apply a small systematic uncertainty for the correction procedure itself, derived from simulated experiments which applied the correction procedure to measured distributions based on POWHEG. The systematic uncertainties on the inclusive Δy measurement are shown in Table XVI, and the total systematic uncertainty is found to be small compared to the statistical uncertainty.

CDF Run II Preliminary L = 8.7 fb ⁻¹	
Source	Systematic Uncertainty
Background Shape	0.014
Background Normalization	0.011
Parton Showering	0.010
Jet Energy Scale	0.005
Initial and Final State Radiation	0.005
Color Reconnection	0.001
Parton Distribution Functions	0.001
Correction Procedure	0.003
Total Systematic Uncertainty	0.022
Statistical Uncertainty	0.041
Total Uncertainty	0.047

TABLE XVI: Systematic Uncertainties on the parton level Δy measurement.

VII. DIFFERENTIAL CROSS-SECTION AND PARTON LEVEL RESULTS

Applying our correction procedure to the data yields the differential cross-section shown in Figure 20 compared to the standard model POWHEG prediction. We find an inclusive asymmetry of $0.162 \pm 0.041 \pm 0.022$. The $|\Delta y|$ dependence of this distribution is shown in Figure 21, with the differential asymmetry values being summarized in Table XVII. Performing a linear fit to the parton level results, we find a slope $\alpha_{\Delta y} = (30.6 \pm 8.6) \times 10^{-2}$, compared to an expected slope of 10.3×10^{-2} . In performing this fit in the data, we utilize the full covariance matrix for the corrected A_{FB} values when minimizing χ^2 in order to account for the correlations between bins in the parton level distribution. The systematic uncertainties on A_{FB} in each bin are added to the diagonals of the covariance matrix.

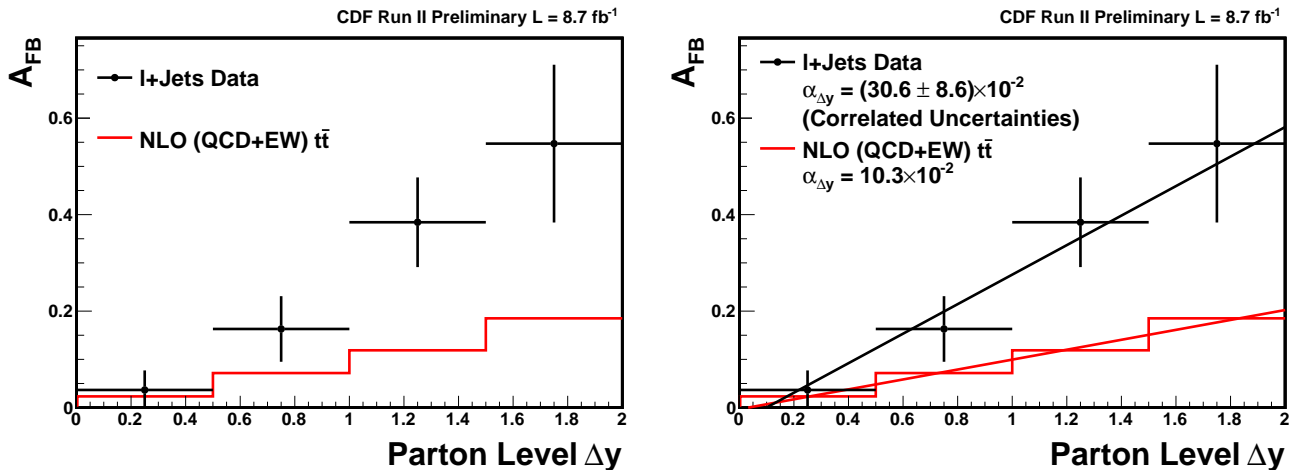


FIG. 21: Parton level A_{FB} as a function of $|\Delta y|$ (left) and the same distribution with a best-fit line superimposed (right).

CDF Run II Preliminary L = 8.7 fb ⁻¹		
Parton Level	Data	NLO (QCD+EW) $t\bar{t}$
$ \Delta y $	$A_{\text{FB}} (\pm \text{stat.} \pm \text{syst.})$	A_{FB}
Inclusive	$0.162 \pm 0.041 \pm 0.022$	0.066
< 0.5	$0.037 \pm 0.035 \pm 0.020$	0.023
0.5 – 1.0	$0.163 \pm 0.058 \pm 0.036$	0.072
1.0 – 1.5	$0.384 \pm 0.084 \pm 0.041$	0.119
≥ 1.5	$0.547 \pm 0.140 \pm 0.085$	0.185
< 1.0	$0.088 \pm 0.042 \pm 0.022$	0.043
≥ 1.0	$0.433 \pm 0.097 \pm 0.050$	0.139
	Data	NLO (QCD+EW) $t\bar{t}$
Slope $\alpha_{\Delta y}$ of Best-Fit Line	$(30.6 \pm 8.6) \times 10^{-2}$	10.3×10^{-2}

TABLE XVII: Measured and predicted parton level asymmetries as a function of $|\Delta y|$.

We also can determine the parton level mass dependence of A_{FB} by correcting the Δy and $M_{t\bar{t}}$ distributions simultaneously. Doing so yields the $M_{t\bar{t}}$ distributions for forward and backward events shown in Figure 22. These distributions can then be combined to determine the differential A_{FB} as a function of $M_{t\bar{t}}$ shown in Figure 23 and summarized in Table XVIII. The best fit line to the parton level data has a slope $\alpha_{M_{t\bar{t}}} = (15.6 \pm 5.0) \times 10^{-4}$, compared to the POWHEG prediction of 3.3×10^{-4} .

A. Comparison to Previous Results

In the 5.3 fb^{-1} version of this analysis, parton level differential asymmetries were considered in two bins of $|\Delta y|$ (above and below 1.0) and two bins of $M_{t\bar{t}}$ (above and below $450 \text{ GeV}/c^2$). In Table XIX, we provide the parton

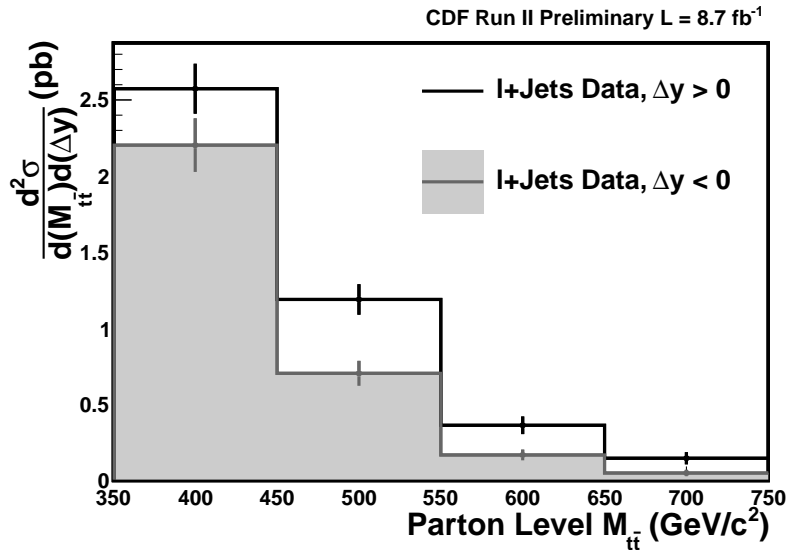


FIG. 22: Parton level $M_{t\bar{t}}$ distributions for events with positive and negative Δy .

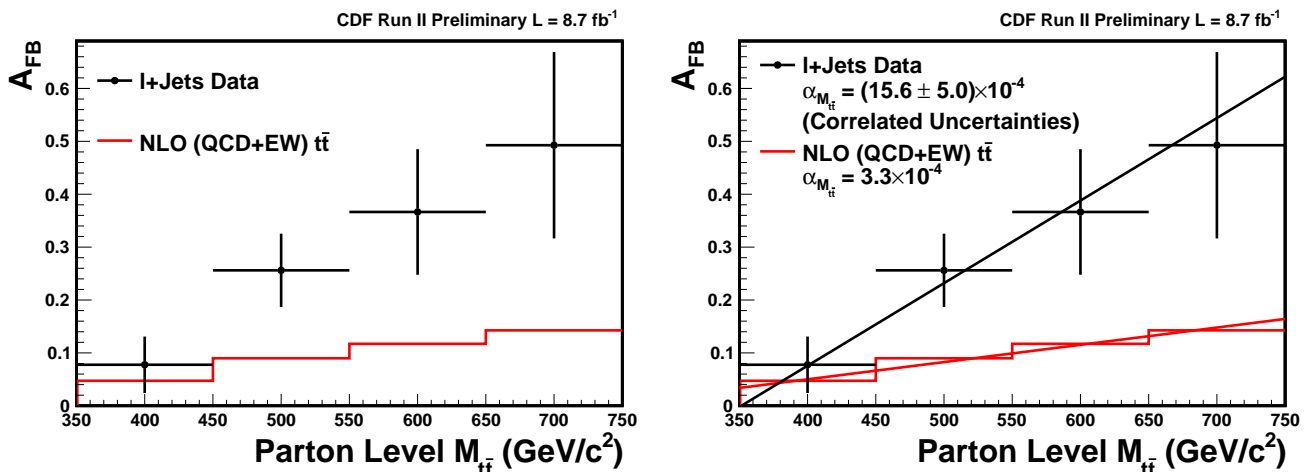


FIG. 23: Parton level A_{FB} as a function of $M_{t\bar{t}}$ (left) and the same distribution with a best-fit line superimposed (right).

level results from this analysis with the same divisions into two bins in order to directly compare to the previous analysis. The change in central values across the two bins has been reduced somewhat compared to the previous analysis, but the trend of growth of the asymmetry with mass and $|\Delta y|$ remains.

VIII. CONCLUSIONS

We have studied the forward-backward asymmetry A_{FB} in top quark pair production in the full CDF dataset. In the full dataset, we observe a raw asymmetry of 0.066 ± 0.020 , and an approximately linear dependence on both $|\Delta y|$ and $M_{t\bar{t}}$. After subtracting off the predicted background contribution, we determine the significance of the rapidity and mass dependence by comparing the best fit slopes in the data to the standard model POWHEG prediction, finding a p-value of 0.00892 for A_{FB} as a function of $|\Delta y|$ and a p-value of 0.00646 for A_{FB} as a function of $M_{t\bar{t}}$. Finally, we correct our results to the parton level to find the differential cross-section in Δy and allow

CDF Run II Preliminary L = 8.7 fb ⁻¹		
Parton Level	Data	NLO (QCD+EW) $t\bar{t}$
$M_{t\bar{t}}$	$A_{\text{FB}} (\pm \text{stat.} \pm \text{syst.})$	A_{FB}
$< 450\text{GeV}/c^2$	$0.078 \pm 0.048 \pm 0.024$	0.047
$450 - 550\text{GeV}/c^2$	$0.256 \pm 0.063 \pm 0.028$	0.090
$550 - 650\text{GeV}/c^2$	$0.366 \pm 0.085 \pm 0.083$	0.117
$\geq 650\text{GeV}/c^2$	$0.493 \pm 0.159 \pm 0.076$	0.143
$< 450\text{GeV}/c^2$	$0.078 \pm 0.048 \pm 0.024$	0.047
$\geq 450\text{GeV}/c^2$	$0.296 \pm 0.059 \pm 0.031$	0.100
	Data	NLO (QCD+EW) $t\bar{t}$
Slope $\alpha_{M_{t\bar{t}}}$ of Best-Fit Line	$(15.6 \pm 5.0) \times 10^{-4}$	3.3×10^{-4}

TABLE XVIII: Measured and predicted parton level asymmetries as a function of $M_{t\bar{t}}$.

CDF Run II Preliminary L = 8.7 fb ⁻¹			
Parton Level	NLO (QCD+EW) $t\bar{t}$	5.3 fb ⁻¹	8.7 fb ⁻¹
$ \Delta y $	A_{FB}	$A_{\text{FB}} (\pm[\text{stat.}+\text{syst.}])$	$A_{\text{FB}} (\pm[\text{stat.}+\text{syst.}])$
Inclusive	0.066	0.158 ± 0.074	0.162 ± 0.047
< 1.0	0.043	0.026 ± 0.118	0.088 ± 0.047
≥ 1.0	0.139	0.611 ± 0.256	0.433 ± 0.109
Parton Level	NLO (QCD+EW) $t\bar{t}$	5.3 fb ⁻¹	8.7 fb ⁻¹
$M_{t\bar{t}}$	A_{FB}	$A_{\text{FB}} (\pm[\text{stat.}+\text{syst.}])$	$A_{\text{FB}} (\pm[\text{stat.}+\text{syst.}])$
$< 450\text{GeV}/c^2$	0.047	-0.116 ± 0.153	0.078 ± 0.054
$\geq 450\text{GeV}/c^2$	0.100	0.475 ± 0.112	0.296 ± 0.067

TABLE XIX: Differential parton level asymmetries compared to the 5.3 fb⁻¹ analysis.

direct comparison with theoretical predictions, finding an inclusive parton level asymmetry of 0.162 ± 0.047 and a linear mass dependence $A_{\text{FB}}(M_{t\bar{t}})$ with slope $(15.6 \pm 5.0) \times 10^{-4}$ compared to the 3.3×10^{-4} in the NLO standard model.

-
- [1] L. G. Almeida, G. F. Sterman and W. Vogelsang, Phys. Rev. D **78**, 014008 (2008); O. Antunano, J. H. Kuhn, and G. V. Rodrigo, Phys. Rev. D **77**, 014003 (2008); M. T. Bowen, S. D. Ellis, and D. Rainwater, Phys. Rev. D **73**, 014008 (2006).
- [2] T. Aaltonen *et al.* (CDF Collaboration), Phys. Rev. Lett. **83**, 112003 (2011); arXiv:1101.0034.
- [3] CDF Collaboration, www-cdf.fnal.gov/physics/new/top/2011/DilAfb/cdfpubnote.pdf, CDF Note 10436 March 2011.
- [4] CDF Collaboration, www-cdf.fnal.gov/physics/new/top/2011/AfbComb/Afb.combo.5invfb.pdf, CDFNote 10584, July 2011.
- [5] V. M. Abazov *et al.* (D0 Collaboration), Phys. Rev. Lett. **84**, 112005 (2011); arXiv:1107.4995.
- [6] Some recent reviews: M. Gresham, I. W. Kim, K. Zurek, arXiv:1102.0018 and Q.-H. Cao, D. McKeen, J. Rosner, G. Shaughnessy, and C. Wagner, Phys. Rev. D **81**, 114004 (2010).
- [7] S. Frixione, P. Nason, and G. Ridolfi, J. High Energy Phys. 0709 (2007) 126.
- [8] S. Frixione and B. R. Webber, J. High Energy Phys. 06 (2002) 029.
- [9] J. M. Campbell, R. K. Ellis, Phys. Rev. D **60**, 113006 (1999).
- [10] W. Hollik and D. Pagani, Phys. Rev. D **84**, 093003 (2011) [arXiv:1107.2606 [hep-ph]].
- [11] J. H. Kuhn and G. Rodrigo, JHEP **1201**, 063 (2012) [arXiv:1109.6830 [hep-ph]].
- [12] A. V. Manohar and M. Trott, arXiv:1201.3926 [hep-ph].
- [13] P. Nason, S. Dawson and R. K. Ellis, Nucl. Phys. B **327**, 49 (1989) [Erratum-ibid. B **335**, 260 (1990)].
- [14] J. Allwall *et al.*, J. High Energy Phys. 09 (2007) 028. We are indebted to T. Tait for the MADGRAPH implementation of

the color-octet models.

- [15] T. Sjostrand, S. Mrenna, and P. Skands, *J. High Energy Phys.* 05 (2006) 026.
- [16] D. Acosta *et al.* (CDF Collaboration), *Phys. Rev. D* **71** 032001 (2005); The CDF II Detector Technical Design Report, FERMILAB-PUB/390-E (1996).
- [17] The charge-conjugate states are implied.
- [18] D. Acosta *et al.* (CDF Collaboration), *Phys. Rev. D* **71** 052003 (2005).
- [19] M.L. Mangano *et al.*, *J. High Energy Phys.* 0307 (2003) 001.
- [20] L. G. Almeida, G. F. Sterman and W. Vogelsang, *Phys. Rev. D* **78**, 014008 (2008);
- [21] A. Höcker and V. Kartvelishvili, *NIM A* **372**, 469 (1996).
- [22] T. Adye, RooUnfold Software Package. hepunix.rl.ac.uk/~adye/software/unfold/RooUnfold.html